solids

MDPI

Article

Mechanical Alloying and Concentration Quenching of the Luminescence of Pr^{3+} Ions in Chalcogenide Glass

Andrey Tverjanovich [1,*], Alexandra Mikhaylova [2] and Eugene Bychkov [3,*]

[1] Institute of Chemistry, St. Petersburg State University, 198504 St. Petersburg, Russia
[2] Centre for Optical and Laser Materials Research, St. Petersburg State University, 198504 St. Petersburg, Russia; alexandra.mikhaylova@spbu.ru
[3] Laboratoire de Physico-Chimie de l'Atmosphère, Université du Littoral Côte d'Opale, 59140 Dunkerque, France
* Correspondence: andr.tver@yahoo.com (A.T.); eugene.bychkov@univ-littoral.fr (E.B.)

Abstract: The disadvantage of chalcogenide glasses containing rare earth ions as luminescent materials for the IR optical range is the strong concentration quenching of luminescence due to the non-uniform distribution of rare earth ions in the glass matrix. This study investigates the effect of grinding chalcogenide glass containing Pr^{3+} ions in a planetary ball mill on its luminescent properties in the near-IR range, as well as its optical properties and structure. The results indicate that milling, under certain conditions, leads to a decrease in the concentration quenching of the luminescence of Pr^{3+} ions. This finding suggests that milling can be used in the development of glassy materials with the increased efficiency of luminescence of rare earth ions. However, it is essential to consider that high-energy milling may result in the formation of areas with increased pressure in the obtained material, leading to structural changes in the glass.

Keywords: chalcogenide glasses; mechanical alloying; concentration quenching; REI luminescence

check for updates

Citation: Tverjanovich, A.; Mikhaylova, A.; Bychkov, E. Mechanical Alloying and Concentration Quenching of the Luminescence of Pr^{3+} Ions in Chalcogenide Glass. *Solids* **2024**, *5*, 292–302. https://doi.org/10.3390/solids5020019

Academic Editor: Michael Reshchikov

Received: 21 March 2024
Revised: 6 May 2024
Accepted: 15 May 2024
Published: 29 May 2024

Copyright: © 2024 by the authors. Licensee MDPI, Basel, Switzerland. This article is an open access article distributed under the terms and conditions of the Creative Commons Attribution (CC BY) license (https://creativecommons.org/licenses/by/4.0/).

1. Introduction

Chalcogenide glasses containing rare earth ions (REIs) have recently been intensively studied as active optical materials for mid-IR fiber optics [1,2] for remote sensing of gases and chemical pollutants. This interest also arises from the fact that this spectral region contains characteristic vibrations of most biomolecules, making it relevant for biomedical applications [3,4]. In this regard, research continues laser generation in chalcogenide glasses containing REIs and fibers based on them. Thus, relatively recently, the promise of chalcogenide glasses containing Pr^{3+} ions as a material with generation laser radiation in the mid-IR spectral region has been demonstrated [5,6]. The efficiency of luminescence depends, among other factors, on the distribution of rare earth (RE) elements within the glass matrix. In chalcogenide glasses, REIs tend to form clusters, leading to non-radiative energy exchange between REIs. This process reduces the lifetime of excited states, the probability of radiative relaxation, and, ultimately, the luminescence efficiency. This mechanism of concentration quenching leads to the fact that, relatively effectively, from the point of view of luminescence, RE elements can be introduced into chalcogenide glasses in concentrations of less than 1 at.%. However, with a uniform distribution of ions in the glass matrix, concentration quenching should occur at RE concentrations of more than 6 at.% [7]. Consequently, the challenge arises from enhancing the homogeneity of RE element distribution within the chalcogenide glass matrix. It was previously shown that chalcogenide glasses can be successfully obtained by the mechanical alloying method from elementary substances [8,9]. This technique has been employed to obtain glassy compositions that are challenging to achieve through conventional melt quenching techniques [10,11]. For example, such a technique has been applied for the preparation of glassy chalcogenide superionic solid electrolytes [12,13]. Thus, one potential solution to address the non-uniform distribution of

REIs in the glass matrix is the mechanical grinding of REI-containing glass in a planetary mill, followed by sample molding through pressing and subsequent sintering. Given the above facts, the objective of this study was to examine the impact of glass grinding in a ball mill under different conditions on the luminescent properties and structure of chalcogenide glass with varying REI contents. As a result of research, it has been shown that milling leads to an increase in the degree of homogeneity in the distribution of Pr^{3+} ions in glass, as evidenced by a shift in concentration quenching to the region of higher REI concentrations. At the same time, the structure of the glass itself also changes.

2. Materials and Methods

2.1. Materials

The synthesis of glasses with the composition $41.39GeS_2$-$30.01GaS_{1.5}$-$28.60SbS_{1.5}$ containing 0, 0.1, 0.3, 0.6, 0.9, and 1.2 at.% Pr was conducted in two stages. Initially, the glass matrix with the composition $41.39GeS_2$-$30.01GaS_{1.5}$-$28.60SbS_{1.5}$ was synthesized. Subsequently, an appropriate amount of Pr was added to the synthesized glass, and the synthesis process was repeated. The syntheses were performed using high-purity elements at 1.3×10^{-2} Pa and sealed in quartz ampoules in a rocking furnace. Chemically pure Pr (Sigma-Aldrich, Saint Louis, MO, USA PN 263176) was used for the synthesis. At the first stage, the synthesis was carried out for the initial 5 h at a temperature of 550 °C to prevent the ampoules from exploding due to high sulfur vapor pressure. Subsequently, the temperature was raised to 800 °C, and the synthesis was continued for another 5 h. After this, the ampoules were heated to a temperature of 950 °C, at which they were kept for an additional 4 h. The melts in the ampoules were then cooled in air from the maximum synthesis temperature. At the second stage of the synthesis, the temperature was immediately increased to 950 °C and held there for 5 h with continuous stirring due to the furnace rocking. After this, the melts in the ampoules were also cooled in air from the maximum synthesis temperature.

The absence of crystalline inclusions was monitored using X-ray diffraction. An example of the X-ray diffraction pattern of glass with 0.6 at.% Pr is shown in Supplementary Material (SM) Figure S1.

Spectral studies of the initial bulk glasses were conducted on polished plane-parallel samples. The photo image of the synthesized glass is shown in Figure 1.

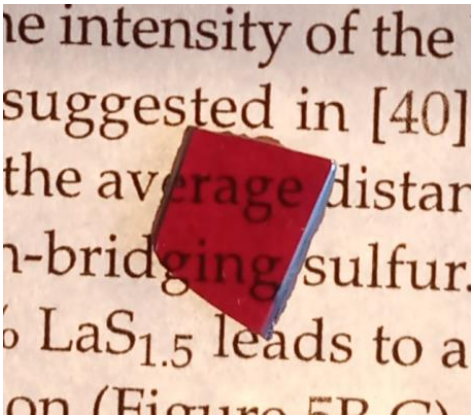

Figure 1. Photo image of the glass with 0.9 at.% Pr placed on paper with the printed text.

To mill the synthesized glasses, a PM 100 planetary ball mill (Retch, Haan, Germany) with a 12 mL stainless steel jar containing 50 balls with a diameter of 5 mm was used. The glasses were pre-ground in an agate mortar. The weight of the glass sample for grinding was approximately 1.5 g. The jar with the prepared grinding glass and balls was filled with argon and hermetically sealed. Milling was carried out in two modes: for 2 h, at a rotation speed of 200 rpm, and for 3 h, at a rotation speed of 500 rpm. Every 30 min, the direction of rotation changed with a pause of 2 min.

To carry out the spectral studies of luminescence, the resulting powders were compacted into pellets using a vacuum mold with an inner diameter of 13 mm (pressure of 550 MPa). The thickness of the pellets was about 2 mm.

The particle size distribution in the resulting powders was found to be wide. The maximum distribution at a rotation speed of 200 rpm occurs at approximately 500 nm. At a rotation speed of 500 rpm, the maximum distribution shifts occur for sizes less than 100 nm. SEM images of the surface of pressed powder pellets obtained are shown in Figure 2. SEM-EDS elemental analysis of the sample after milling, performed at several points, showed the same Pr content, which may indicate its uniform distribution in the sample. The results of the analysis are shown in Figure S2 and Table S1 of Supplementary Materials.

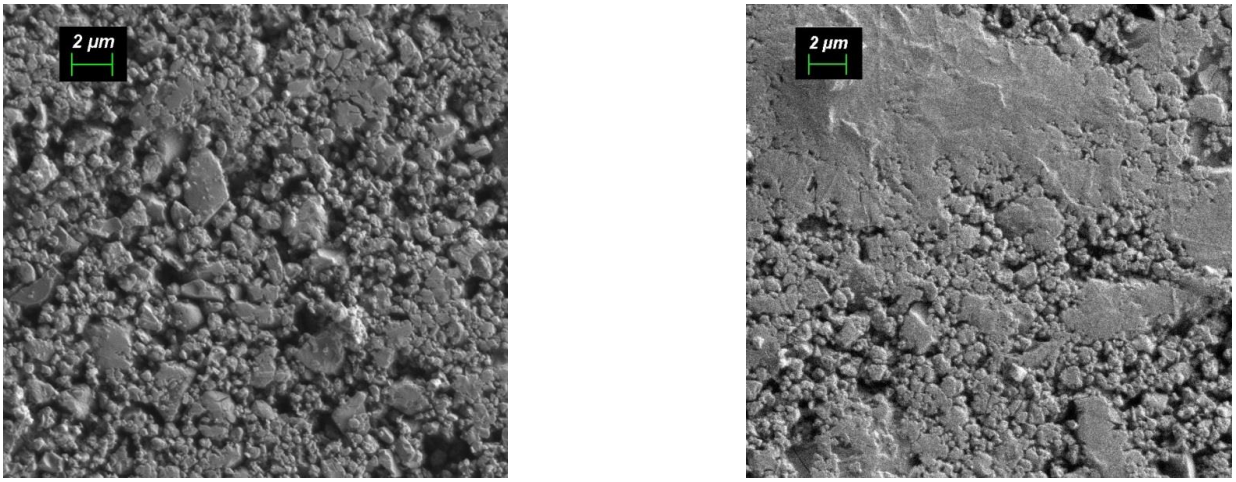

(**a**) (**b**)

Figure 2. SEM images of the surface of a pellet pressed from glass powder containing 0.6 at.% Pr, prepared by milling for 2 h at a rotation speed of 200 rpm (**a**) or for 3 h at a rotation speed of 500 rpm (**b**).

2.2. Methods

The optical absorption spectra of the initial monolithic glasses were measured on a UV-3600 spectrophotometer (Shimadzu, Kyoto, Japan). The spectral dependence of the diffuse reflectance of the powders was measured on a Lambda 1050 spectrophotometer (Perkin Elmer, Waltham, MA, USA) equipped with a 150 mm InGaAs integrating sphere.

Luminescence spectra were measured using a Fluorolog-3 spectrofluorimeter (Horiba Scientific (Jobin Yvon), Osaka, Japan) in the spectral range of 700 to 1500 nm. The pump radiation was directed at the sample's surface at an angle of approximately 90°. A light guide to collect the luminescence signal was positioned at an angle of approximately 45° to this surface and at a distance of about 2 cm from the sample surface to prevent the reflected pump beam from entering the light guide. To determine the most effective luminescence excitation wavelength, the luminescence excitation spectrum was measured at a wavelength of 1040 nm. The spectrum is shown in Figure S3 (Supplementary Materials). Subsequently, the pump radiation wavelength determined in this way (607 nm) was used to excite luminescence.

Raman spectra of glassy samples were measured on a Senterra Raman spectrometer (Bruker, Billerica, MA, USA) with a BX-52 optical microscope with 10× lens (Olympus, Tokyo, Japan) at room temperature. A laser with a wavelength of 785 nm served as the excitation source. The measurements were carried out at a laser radiation power of 1 mW to prevent heating of the samples.

To estimate the size of glass particles after milling, images of the surface of pressed powder pellets were obtained using a SEM Supra 40VP (Zeiss, Jena, Germany). Elemental analysis of the sample was carried out using INCAx-act x-ray microanalysis attachment (Oxford Instruments, Abingdon, England) to SEM Merlin (Zeiss, Jena, Germany).

3. Results and Discussion

3.1. Luminescence Properties

In order to compare the luminescence intensity of samples with different Pr^{3+} contents, measurements were carried out under identical conditions. A protective mask was applied to the samples, enabling the standardization of the area of illumination and collection of the optical signal. Thus, luminescence spectra were obtained for both the original monolithic glasses before milling and the pressed powders after milling. Figure 3 shows the luminescence spectra of glasses with different contents of Pr^{3+} ions after milling at a rotation speed of 200 rpm for 2 h.

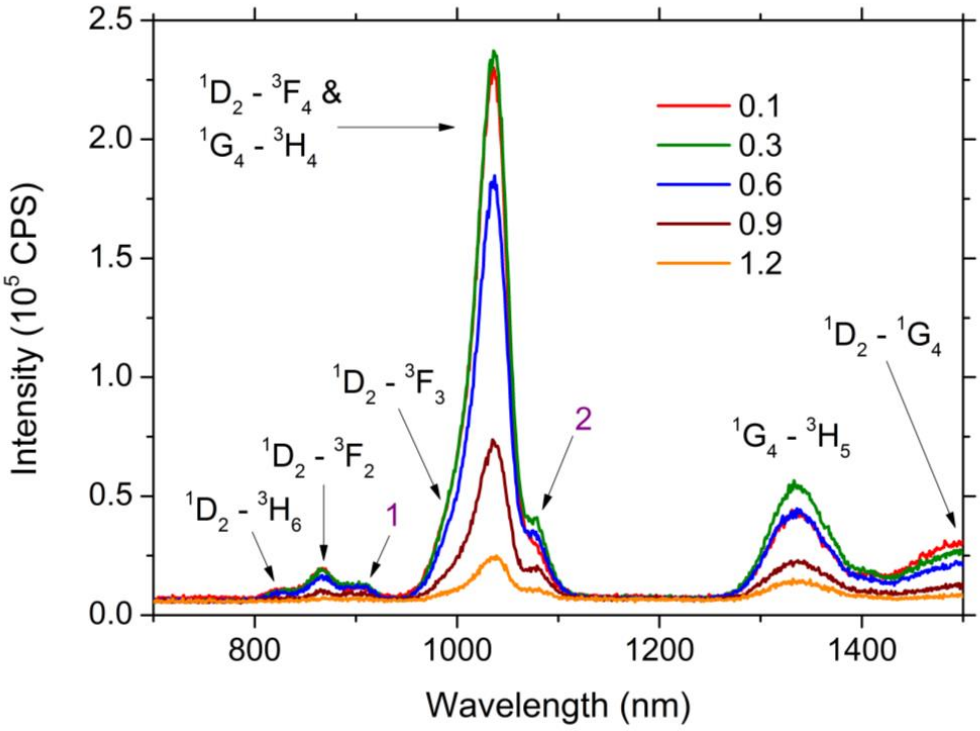

Figure 3. Luminescence spectra of glasses with different contents of Pr^{3+} ions after milling in a planetary ball mill at a rotation speed of 200 rpm.

The corresponding diagram of the optical transitions of the Pr^{3+} ion is provided in Figure 4a. The luminescence transitions are marked with orange arrows.

The maximum luminescence intensity is observed for the double transitions $^1D_2$-$^3F_4$ and $^1G_4$-$^3H_4$ in the wavelength region of 1037 nm. The second most intense luminescence peak is observed at the telecommunications wavelength of 1336 nm, caused by the $^1G_4$-$^3H_5$ transition. The peaks marked in Figure 3 by numbers 1 and 2 refer to the $^4F_{3/2}$–$^4I_{9/2}$ and $^4F_{3/2}$–$^4I_{11/2}$ transitions of Nd^{3+} impurity ions, respectively [14].

After glass milling, the luminescence spectrum undergoes slight changes. Figure 4b shows the luminescence spectra of glass containing 0.3 at.% Pr before milling and the same glass after grinding at a mill rotation speed of 200 rpm. For a correct comparison, the spectra are normalized to the intensity of the most intense peak located in the region at 1036 nm (corresponding to double transition $^1D_2$-$^3F_4$ and $^1G_4$-$^3H_4$). The main difference in the spectra is a decrease in the relative intensity of the radiative transition in the 1335 nm region ($^1G_4$-$^3H_5$) for the milled glass. This decrease in the probability of a radiative transition from the $^1G_4$ level can be associated with both a decrease in the population of this level and with an increase in the probability of non-radiative relaxation from this level. According to the diagram of praseodymium levels with transitions between them achieved at the used pump wavelength, which is presented in Figure 4a, the $^1G_4$ level is mainly populated due to the $^1D_2$-$^1G_4$ radiative transition. The relative intensity of luminescence corresponding to this transition remains unchanged when the glass is dispersed. Therefore, we will focus

on the non-radiative relaxation of excitation. Non-radiative losses can be caused either by non-radiative relaxation from the $^1G_4$ level to the $^3F_4$ level or by the possibility of a process of energy transfer with increasing frequency $^1G_4$-$^3H_5$ with $^1G_4$-$^1D_2$ as assumed in [15]. However, the rather large difference in the energies of the transitions $^1G_4$-$^3H_5$ (7636 cm^{-1}) and $^1G_4$-$^1D_2$ (6865 cm^{-1}) casts doubt on the effectiveness of this process. The mechanism responsible for non-radiative relaxation from the $^1G_4$ level to the $^3F_4$ level may be multiphonon relaxation. The probability of multiphonon relaxation is primarily determined by the number of phonons required to cover the energy required for such a transition. Thus, the rate of multiphonon relaxation is determined by the following expression [16]:

$$W_{ph} = C\left[\left(e^{\left(\frac{h\nu}{KT}\right)} - 1\right)^{-1} + 1\right]^{p} \exp(-\alpha \Delta E) \quad (1)$$

where parameters C and α depend only on the matrix of the glass, p is the number phonons required to overlap the energy gap ΔE, and $h\nu$ is the phonon energy.

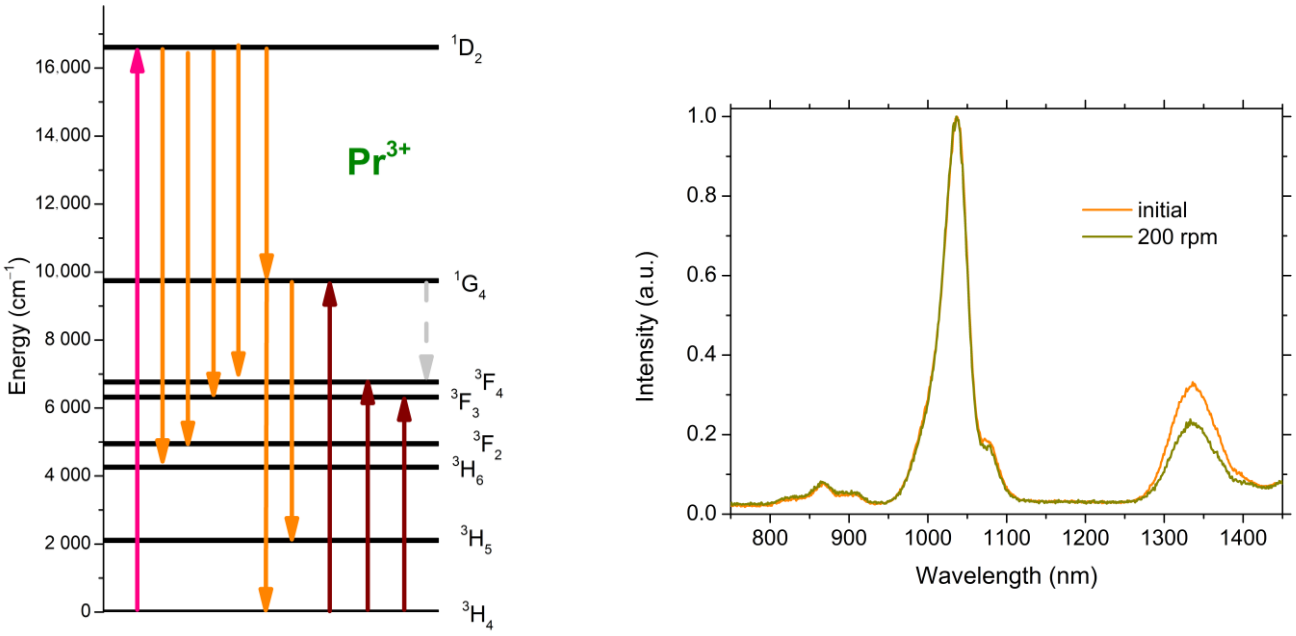

(**a**) (**b**)

Figure 4. (**a**) Optical transitions corresponding to the luminescence and absorption spectra. The crimson arrow represents luminescence pump radiation. Orange arrows indicate luminescence transitions, while brown arrows represent absorption transitions. The gray dashed line signifies non-radiated relaxation. (**b**) Luminescent spectra of the glass with 0.3 at.% Pr before and after milling at a rotation speed of 200 rpm.

The energy gap between the $^1G_4$ and $^3F_4$ levels is 2981 cm^{-1}. For the glass under study, the highest energy phonon mode is the vibration of edge-sharing tetrahedra $GeS_{4/2}$ with the vibration energy of 430 cm^{-1}. In the Raman spectrum of glass, which will be discussed later, this vibration corresponds to a shoulder. Thus, for such relaxation, it is necessary to involve seven phonons. However, if the proportion of non-stoichiometric sulfur–sulfur bonds with phonon energy of 485 cm^{-1} in the glass increases, then, six phonons are required. In this case, according to expression (1), the probability of non-radiative losses from the $^1G_4$ level will increase significantly, and the probability of a radiative transition will decrease. Thus, increasing the fraction of sulfur–sulfur bonds should lead to an increase in the probability of non-radiative relaxation, thereby reducing the probability of the $^1G_4$-$^3H_5$ radiative transition. Furthermore, in the section devoted to changes in the structure of

glass under the influence of dispersion, it will be shown that the proportion of homobonds actually increases with dispersion.

The dependence of the luminescence intensity at a wavelength of 1037 nm on the content of Pr^{3+} ions, corresponding to the data presented in Figure 3, is shown in Figure 5. According to the data, an increase in the concentration of Pr^{3+} ions in the glass by more than 0.1–0.3 at.% leads to a decrease in luminescence intensity. This indicates a significantly non-uniform distribution of Pr^{3+} ions in the glass matrix, despite the milling process. As previously mentioned, with a uniform distribution of REIs in the glass matrix, concentration quenching should be observed at REI concentrations of more than 6 at.%. Moreover, comparing this result with a similar dependence obtained for the initial bulk glass, presented in the same figure, reveals that the maximum luminescence intensity for the concentration curve is in the same concentration range. Only the relative luminescence intensity of the compositions before and after the maximum increased. Such a change in the shape of the dependence may indicate the formation of microregions with different distributions of RE elements throughout the sample volume during the grinding process. When the degree of grinding was increased by raising the rotation speed of the planetary mill to 500 rpm and extending the milling time to 3 h, the nature of the concentration dependence changed. The luminescence intensity increased as the content of Pr^{3+} ions increased over the entire range of concentrations studied (Figure 5). Thus, under certain conditions, milling can be used to shift concentration quenching towards higher concentrations of REI.

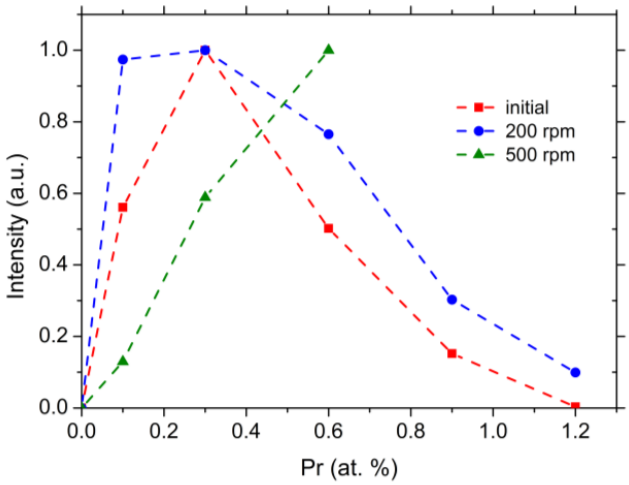

Figure 5. Concentration dependence of the relative luminescence intensity at a wavelength of 1037 nm for the initial bulk glass and glass after milling at speeds of 200 rpm and 500 rpm.

3.2. Structure and Optical Properties

To trace structural changes during milling, Raman spectra of glass samples with different Pr contents were measured before and after milling. The Raman spectra of the initial bulk glass with different Pr contents are shown in Figure 6a.

With an increase in the Pr^{3+} content in the initial glass, there is a monotonic increase in the scattering intensity in the vicinity of 166 and 209 cm^{-1}, and in the range from 270 to 426 cm^{-1}, with a dip around 340 cm^{-1}. This trend is clearly visible in the difference spectrum of glasses with different Pr contents and the initial glass without Pr (Figure 6b). The band in the 166 cm^{-1} region can be attributed to vibrations of Sb-Sb bonds [17,18]. The band in the region of 210 cm^{-1} may indicate the presence of Sb-Ge(Ga) chemical bonds [18,19]. This Raman shift value is also characteristic of lanthanide sulfides [20], but in this case, the Pr concentration is too low for such an effect. The band in the region of 342 cm^{-1} is due to the fully symmetric vibration of $GeS_{4/2}$ tetrahedra [21]. Thus, it can be assumed that the introduction of Pr into the glass, due to the high coordination of Pr, leads to the redistribution of sulfur between metal atoms (ions) and the formation of non-stoichiometric Sb-Sb(Ge,Ga) bonds. The increase in scattering intensity around 342 cm^{-1} is

apparently associated with broadening of the peaks caused by fully symmetric vibrations of the main structural units that form the structure of the glass matrix, namely, $GeS_{4/2}$, $GaS_{4/2}^{-}$, and $SbS_{3/2}$, located at 342, 320, and 297 cm^{-1}, respectively [18,21]. The broadening is presumably caused by a distortion of the structural units, namely, an increased variation in the chemical bond angles M-S-M and S-M-S, where M = Sb(Ge,Ga), due to structural disturbance caused by the introduction of the Pr^{3+} ion into the glass matrix, forming an atypically high-coordination environment around itself. Thus, the coordination number in glass for Sb is typically three [22,23], and for Ge and Ga, it is four [23,24]. However, for the lanthanide ion (Pr^{3+}), it ranges from 6 to 9 according to various sources [13,25,26].

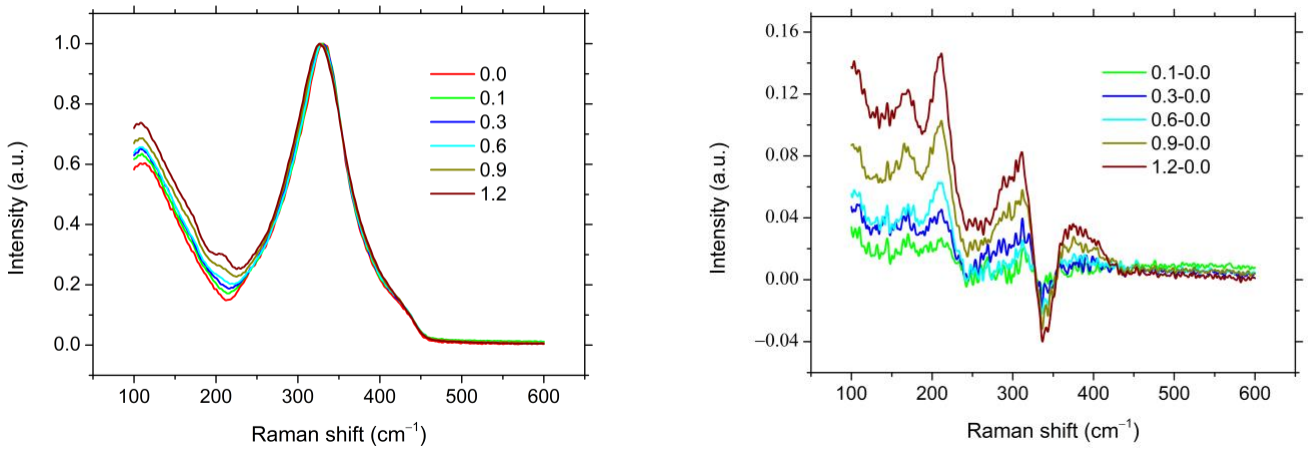

(**a**) (**b**)

Figure 6. (**a**) Raman spectra of initial bulk glasses containing from 0 to 1.2 at.% Pr. (**b**) Results of subtracting the Raman spectrum for glass without RE element from the Raman spectra for glasses with different contents of Pr^{3+} ions.

The milling process does not result in a fundamental change in the glass structure. The Raman spectra of glasses after milling correspond to the spectra of the initial bulk glasses. Figure 7a displays the Raman spectra of glasses containing 0.6 at.% Pr, including both the initial bulk glass and samples after milling at rotation speeds of 200 and 500 rpm.

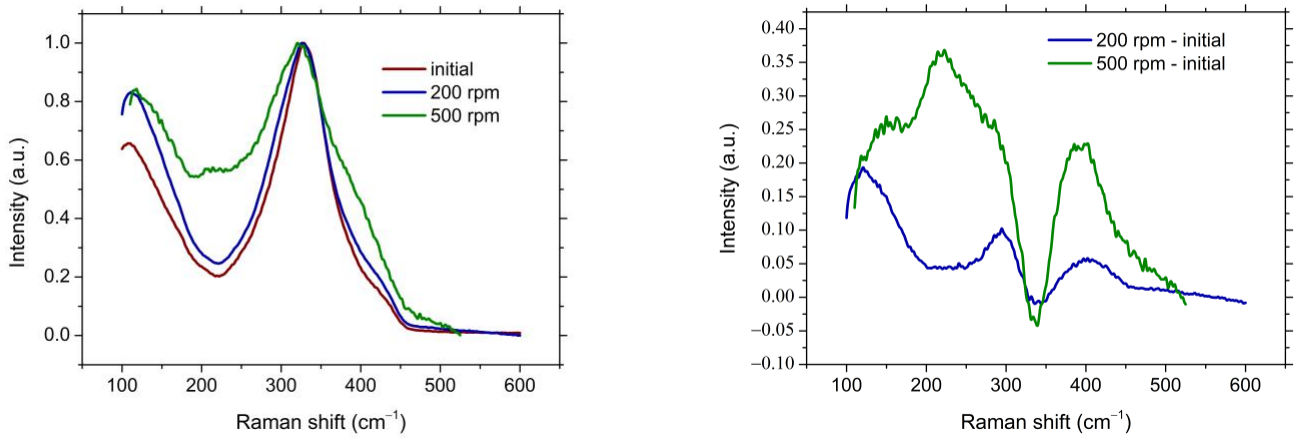

(**a**) (**b**)

Figure 7. (**a**) Raman spectra of glass with 0.6 at.% Pr before and after milling at rotation speeds of 200 and 500 rpm. (**b**) The result of subtracting the Raman spectrum of glass with 0.6 at.% Pr before milling from the Raman spectra of the same glass samples after milling at rotation speeds of 200 and 500 rpm.

An increase in the scattering intensity for the milled sample in the region of 300 and 400 cm^{-1} (refer to the difference spectrum of the initial glass and that milled at a speed of 200 rpm shown in Figure 7b) may result from the broadening of the main peaks with an increase in the concentration of defective structural units that form the glass structure. This process is attributed to mechanical impact. The increase in intensity in the low-frequency region remains unclear. It could be attributed either to an increase in the intensity of the Boson peak or to specific changes in deformation vibrations of chemical bonds.

The Boson peak is characteristic of the amorphous state and is caused by the collective motions of atoms within the medium-ranged structural order. An increase in the intensity of the Boson peak is also observed when Pr^{3+} ions are introduced into the glass (Figure 6a). It was previously assumed that, in glasses containing REIs, the Boson peak is determined by structural correlations caused by non-bridging anions, in this case, non-bridging sulfur [27]. However, this issue requires more detailed research.

When glasses were milled at a rotation speed of 500 rpm, the structure of the glass underwent much larger changes, clearly visible in the Raman spectra, and especially in the difference Raman spectra. In addition to enhancing the changes observed for the sample obtained at a speed of 200 rpm, additional features appear in the spectrum. Noteworthily, additional scattering is evident in the region of 220 cm^{-1} and 490 cm^{-1}. Hence, along with stronger distortions of the structure (changes in the bond angles S-M-S and M-S-M, where M = Ge, Ga, Sb), leading to the broadening of the peaks, an increase in the fraction of non-stoichiometric Sb-Ge(Ga) (220 cm^{-1} [18,19]) and S-S (490 cm^{-1} [28]) bonds is observed. The increase in the fraction of homopolar M-M bonds during the milling process is consistent with the shift of the fundamental absorption edge of glass to the long-wavelength range of the spectrum as a result of milling. This shift is clearly visible when comparing the optical absorption spectra of glass before and after milling (Figure 8). The experimental data on diffuse reflection $R(\lambda)$ of the powder were converted into optical absorption coefficient $\alpha(\lambda)$ following the Kubelka–Munk equation [29].

$$\frac{(1-R(\lambda))^2}{R(\lambda)} \sim \alpha(\lambda) \quad (2)$$

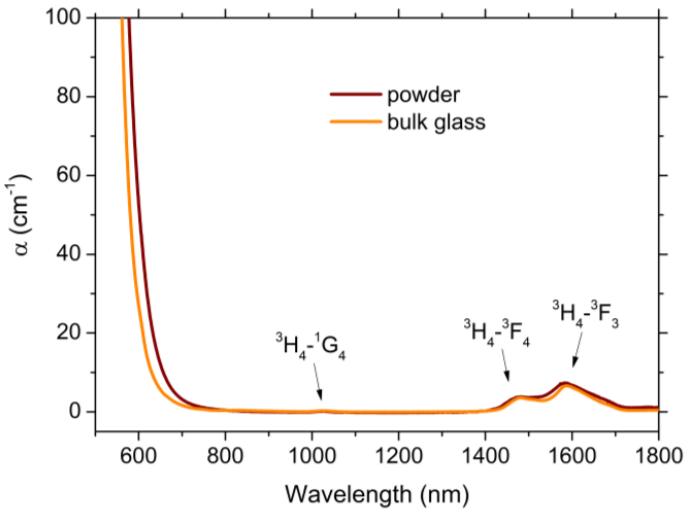

Figure 8. Optical absorption spectrum of bulk glass with 0.6 at.% Pr and after its milling at a rotation speed of 500 rpm.

The proportionality coefficient in this equation was determined from the condition of equality of the optical absorption coefficient corresponding to the $^3H_4$-$^3F_3$ transition of the Pr^{3+} ion in bulk glass and the powder of the same glass.

The optical transitions corresponding to the absorption peaks observed in Figure 8 are indicated in Figure 4 by brown arrows.

The increase in the proportion of homopolar bonds is apparently caused by the occurrence of dissociation reactions, for example, $GeS_2 \leftrightarrow Ge + 2S$ and/or disproportionation reactions $GeS_2 \leftrightarrow GeS + S$. Similar changes, namely, a shift absorption edge to longer wavelengths and an increase in the fraction of homopolar bonds, were observed in the Raman spectrum of GeS_2 glass after applying a pressure of 8.3 GPa [30]. It can be assumed that the structure of the glass during milling is distorted not only in the surface layer of the resulting particles but also, due to pressure, in deeper layers. The magnitude of this pressure is quite large. This conclusion is consistent with the results of other studies on the effect of the milling process on the structure of the material. For example, it was shown that the high-pressure phase In_2O_3 (hexagonal h-In_2O_3), which exists at ambient temperatures only at a pressure above 15.3 GPa or at $T \gtrsim 1000$ °C and $P \gtrsim 6.5$ GPa, can be obtained by milling a cubic modification c-In_2O_3 (that is stable under ambient conditions) in a planetary ball mill [31].

The results obtained suggest that further research into developing methods of mechanical milling of chalcogenide glasses doped with RE elements and their subsequent sintering using, for example, Spark Plasma Sintering (SPS) technology [9], will make it possible to obtain glasses with significantly increased luminescence efficiency. Based on these glasses, optically active fibers for the IR range can be fabricated.

4. Conclusions

The glasses of the composition $41.39GeS_2$-$30.01GaS_{1.5}$-$28.60SbS_{1.5}$, containing 0, 0.1, 0.3, 0.6, 0.9, and 1.2 at.% Pr^{3+}, were investigated. The influence of their grinding in a planetary ball mill at rotation speeds of 200 and 500 rpm on their luminescent properties in the near-IR range, as well as their structure and optical properties, were studied. It has been shown that, at a rotation speed of 200 rpm, the structure inherent to the initial bulk glass is largely preserved. The fraction of defect states increases slightly, leading to the broadening of the Raman peaks and the broadening of the maximum luminescence intensity of Pr^{3+} ions based on its concentration dependence. Additionally, the relative intensity of Raman scattering increases in the low-frequency region of the spectrum, indicating a potential increase in the intensity of the Boson peak. At a rotation speed of 500 rpm, the glass structure undergoes significantly more pronounced changes. Along with very strong broadening of the Raman peaks, vibration features related to metal–metal and sulfur–sulfur bonds appear. Similar changes are observed in the Raman spectrum of GeS_2 glass at high pressure. Additionally, the degree of homogeneity in the distribution of Pr^{3+} ions in the matrix of the glassy material increases, as evidenced by a shift in concentration quenching to the region of higher REI concentrations. Thus, mechanical alloying can be considered as the method for the development of luminescent materials based on chalcogenide glasses with RE elements, exhibiting increased luminescence efficiency by reducing concentration quenching due to a more uniform distribution of REIs in the glass matrix.

Supplementary Materials: The following supporting information can be downloaded at: https://www.mdpi.com/article/10.3390/solids5020019/s1. Figure S1: X-ray diffraction pattern of the glass with 0.6 at.% Pr. Figure S2: SEM-EDS elemental analysis of Pr in the sample after milling. Figure S3: Excitation spectrum of luminescence at a wavelength of 1040 nm of the glass sample with 0.6 at.% Pr.

Author Contributions: Conceptualization, A.T.; methodology, A.T.; validation, A.T.; formal analysis, A.T.; investigation, A.T. and A.M.; resources, A.T.; data curation, A.T.; writing—original draft preparation, A.T.; writing—review and editing, A.T. and E.B.; visualization, A.T.; supervision, A.T. and E.B.; project administration, A.T.; funding acquisition, A.T. All authors have read and agreed to the published version of the manuscript.

Funding: This work was supported by the Russian Science Foundation under grant no. 22-23-00074, https://rscf.ru/en/project/22-23-00074/ (accessed on 29 January 2021).

Data Availability Statement: Data are contained within the article.

Acknowledgments: A part of the measurements were carried out in the resource centers of St. Petersburg State University: "Centre for Optical and Laser Materials Research"; "Interdisciplinary Resource Centre for Nanotechnology"; and "Center for X-ray diffraction studies".

Conflicts of Interest: The authors declare no conflicts of interest.

References

1. Li, L.; Bian, J.; Jiao, Q.; Liu, Z.; Dai, S.; Lin, C. GeS_2–In_2S_3–CsI Chalcogenide Glasses Doped with Rare Earth Ions for Near- and Mid-IR Luminescence. *Sci. Rep.* **2016**, *6*, 37577. [CrossRef] [PubMed]
2. Yang, Z.; Pan, H.; Chen, Y.; Wang, R.; Shen, X. Emission properties of Er^{3+}-doped Ge20Ga5Sb10Se65 glasses in near- and mid-infrared. *Infrared Phys. Technol.* **2018**, *89*, 277–281. [CrossRef]
3. Anne, M.-L.; Keirsse, J.; Nazabal, V.; Hyodo, K.; Inoue, S.; Boussard-Pledel, C.; Lhermite, H.; Charrier, J.; Yanakata, K.; Loreal, O.; et al. Chalcogenide Glass Optical Waveguides for Infrared Biosensing. *Sensors* **2009**, *9*, 7398–7411. [CrossRef] [PubMed]
4. Mishra, S.; Jaiswal, P.; Lohia, P.; Dwivedi, D.K. Chalcogenide glasses for sensor application: A Review. In Proceedings of the 5th IEEE Uttar Pradesh Section International Conference on Electrical, Electronics and Computer Engineering (UPCON), Gorakhpur, India, 2–4 November 2018; pp. 1–5. [CrossRef]
5. Sójka, L.; Tang, Z.; Furniss, D.; Sakr, H.; Bere's-Pawlik, E.; Seddon, A.B.; Benson, T.M.; Sujecki, S. Numerical and Experimental Investigation of Mid-Infrared Laser Action in Resonantly Pumped Pr^{3+} Doped Chalcogenide Fibre. *Opt. Quantum Electron.* **2017**, *49*, 21. [CrossRef]
6. Churbanov, M.F.; Denker, B.I.; Galagan, B.I.; Koltashev, V.V.; Plotnichenko, V.G.; Snopatin, G.E.; Sukhanov, M.V.; Sverchkov, S.E.; Velmuzhov, A.P. Laser Potential of Pr^{3+} Doped Chalcogenide Glass in 5–6 μm Spectral Range. *J. Non Cryst. Solids* **2021**, *559*, 120592. [CrossRef]
7. Tver'yanovich, Y.S.; Tverjanovich, A. Rare-earth doped chalcogenide glasses. In *Semiconducting Chalcogenide Glass*; Fairman, R., Ushkov, B., Eds.; Elsevier Academic Press: Amsterdam, The Netherlands; San Diego, CA, USA, 2004; pp. 169–207.
8. Petracovschi, E.; Hubert, M.; Adam, J.-L.; Zhang, X.-H.; Calvez, L. Synthesis of $GeSe_4$ glass by mechanical alloying and sintering. *Phys. Status Solidi B* **2014**, *251*, 1330–1333. [CrossRef]
9. Calvez, L.; Lavanant, E.; Novikova, A.; Goncalves, C.; Bureau, B.; Nazabal, V.; Jouan, T.; Zhang, X.-H. Te-As-Se glass destabilization using high energy milling. *J. Non Cryst. Solids* **2018**, *480*, 28–33. [CrossRef]
10. Xie, S.; Gu, J.; Jia, G.; Liu, Z.; Gu, C.; Gao, Y.; Zheng, W.; Liu, Z.; Shen, X.; Chen, Y. Obtaining Ultra-High Hardness in Spark Plasma Sintered $Ge_{40}As_{40}Se_{20}$ Bulk Glass. *SSRN* **2024**. [CrossRef]
11. Dénoue, K.; Le Coq, D.; Calers, C.; Gautier, A.; Verger, L.; Calvez, L. New Synthesis Route for Glasses and Glass-Ceramics in the Ga_2S_3–Na_2S Binary System. *Mater. Res. Bull.* **2021**, *142*, 111423. [CrossRef]
12. Fan, B.; Fu, H.; Li, H.; Xue, B.; Zhang, X.; Luo, Z.; Ma, H. Ionic conductive GeS_2–Ga_2S_3–Li_2S–LiI glass powders prepared by mechanical synthesis. *J. Alloys Compd.* **2018**, *740*, 61–67. [CrossRef]
13. Zhang, J.; Nazabal, V.; Le Coq, D.; Calvez, L.; Zhang, X.-H.; Hernandez, O.; Duplaix-Rata, G.; Poidevin, C.; Rocquefelte, X.; Furet, E.; et al. Ionic Conductivity and Structure of Glasses Synthesized by Mechanical-Milling Methods in the x[Na_2S]-(100-x)[0.5GeS_2-0.5Ga_2S_3] System. *Inorg. Chem.* **2023**, *62*, 19033–19042. [CrossRef] [PubMed]
14. Tverjanovich, A.; Smirnov, E. Peculiarity of the Structure and Luminescence of Glasses in La_2S_3–Ga_2S_3–GeS_2:Pr^{3+} System. *Materials* **2023**, *16*, 7094. [CrossRef] [PubMed]
15. Balda, R.; Mendioroz, A.; Fernandez, J.; Arriandiaga, M.A.; Griscom, L.S.; Adam, J.L. Laser spectroscopy and upconversion studies of Pr+-doped halide modified sulfide glasses. *Opt. Mater.* **2001**, *16*, 249–254. [CrossRef]
16. Layne, C.B.; Lowdermilk, W.H.; Weber, M.J. Multiphonon relaxation of rare-earth ions in oxide glasses. *Phys. Rev. B* **1977**, *16*, 10–20. [CrossRef]
17. Watanabe, I.; Noguchi, S.; Shimizu, T. Study on local structure in amorphous Sb-S films by Raman scattering. *J. Non Cryst. Solids* **1983**, *58*, 35–40. [CrossRef]
18. Tverjanovich, A.; Tveryanovich, Y.S.; Shahbazova, C. Structure and Luminescent Properties of Glasses in the GeS_2–Ga_2S_3–Sb_2S_3:Pr^{3+} System. *Materials* **2023**, *16*, 4672. [CrossRef] [PubMed]
19. Pethes, I.; Nazabal, V.; Ari, J.; Kaban, I.; Darpentigny, J.; Welter, E.; Gutowski, O.; Bureau, B.; Messaddeq, Y.; Jóvári, P. Atomic level structure of Ge–Sb–S glasses: Chemical short range order and long Sb-S bonds. *J. Alloys Compd.* **2019**, *774*, 1009–1016. [CrossRef]
20. Lucazeau, G.; Barnier, S.; Loireau-Lozac'h, A.M. Vibrational spectra, electronic transitions and short order structure of rare earth—Gallium sulphide glasses. *Spec. Acta Part A* **1978**, *34*, 21–27. [CrossRef]
21. Holomb, R.; Johansson, P.; Mitsa, V.; Rosola, I. Local structure of technologically modified g-GeS_2: Resonant Raman and absorption edge spectroscopy combined with ab initio calculations. *Phil. Mag.* **2005**, *85*, 2947–2960. [CrossRef]
22. Kassem, M.; Benmore, C.J.; Tverjanovich, A.; Usuki, T.; Khomenko, M.; Fontanari, D.; Sokolov, A.; Ohara, K.; Bokova, M.; Kohara, S.; et al. Glassy and liquid Sb_2S_3: Insight into the structure and dynamics of a promising functional material. *J. Mater. Chem. C* **2023**, *11*, 4654–4673. [CrossRef]
23. Pethes, I.; Nazabal, V.; Chahal, R.; Bureau, B.; Kaban, I.; Beuneu, B.; Bednarcik, J.; Jóvári, P. The structure of near stoichiometric Ge-Ga-Sb-S glasses: A reverse Monte Carlo study. *J. Non Cryst. Solids* **2019**, *505*, 340–346. [CrossRef]

24. Pethes, I.; Nazabal, V.; Chahal, R.; Bureau, B.; Kaban, I.; Belin, S.; Jóvári, P. Local motifs in GeS_2–Ga_2S_3 glasses. *J. Alloys Compd.* **2016**, *673*, 149–157. [CrossRef]
25. Drewitt, J.W.E.; Salmon, P.S.; Zeidler, A.; Benmore, C.J.; Hannon, A.C. Structure of rare-earth chalcogenide glasses by neutron and x-ray diffraction. *J. Phys. Condens. Matter* **2017**, *29*, 225703. [CrossRef] [PubMed]
26. Choi, Y.G.; Song, J.H. Local structural environment and intra-4f transition of rare-earth ion in chalcogenide glass: Comparison between Dy-doped Ge–As–S and Ge–Ga–S glasses. *J. Non Cryst. Solids* **2009**, *355*, 2396–2399. [CrossRef]
27. Tikhomirov, V.K.; Jha, A.; Perakis, A.; Sarantopoulou, E.; Naftaly, M.; Krasteva, V.; Li, R.; Seddon, A.B. An interpretation of the Boson peak in rare-earth ion doped glasses. *J. Non Cryst. Solids* **1999**, *256–257*, 89–94. [CrossRef]
28. Blaineau, S.; Jund, P. Vibrational signature of broken chemical order in a GeS_2 glass: A molecular dynamics simulation. *Phys. Rev. B* **2004**, *69*, 064201. [CrossRef]
29. Trikalitis, P.N.; Rangan, K.K.; Mercouri, T.B.; Kanatzidis, G. Varied pore organization in mesostructured semiconductors based on the $[SnSe_4]^{4-}$ anion. *Nature* **2001**, *410*, 671–675. [CrossRef] [PubMed]
30. Tverjanovich, A.S.; Tsiok, O.B.; Brazhkin, V.V.; Bokova, M.; Cuisset, A.; Bychkov, E. Remarkably stable Glassy GeS_2 Densified at 8.3 GPa: Hidden Polyamorphism, Contrasting Optical Properties, Raman and DFT Studies, Advanced Applications. *J. Phys. Chem. B* **2023**, *127*, 9850–9860. [CrossRef]
31. Liu, D.; Lei, W.; Qin, S.; Hou, L.; Liu, Z.; Cui, Q.; Chen, Y. Large-Scale Synthesis of Hexagonal Corundum-Type In_2O_3 by Ball Milling with Enhanced Lithium Storage Capabilities. *J. Mater. Chem. A* **2013**, *1*, 5274–5278. [CrossRef]

Disclaimer/Publisher's Note: The statements, opinions and data contained in all publications are solely those of the individual author(s) and contributor(s) and not of MDPI and/or the editor(s). MDPI and/or the editor(s) disclaim responsibility for any injury to people or property resulting from any ideas, methods, instructions or products referred to in the content.